REU Project: Spectral Synthesis via Multi-Loop Convolution of Retracting Thin-Flux Tubes

C. W. Fairbairn
Supervisor: Dana Longcope
Montana State University, Barnard Hall, Bozeman North Haugh, MT, USA

Abstract

Previous work by Longcope et al. [2016] has investigated the use of numerical modelling to synthesise solar flare spectra. In particular they evolved a single Thin-Flux Tube (TFT) after an assumed reconnection event and generated theoretical thermal emission. The TFT initialisation parameters were chosen to fit the resulting spectra to the 2004 February 26$^{\text{th}}$ compact X-class flare RHESSI observed spectra. This method demonstrated a successful fit in the x-ray regime at a particular time during the impulsive phase. However, at later and earlier times this single loop method deviated from observations. This motivates us to re-examine the synthesised spectral evolution by incorporating several loops into a multi-stage convolution. Here different loop types are triggered at different times in order to achieve a better fit. This study has proved effective with a better overall fit across time. We also note that there is a considerable improvement in both GOES channel comparisons. Analysing the temporal changes in loop parameters used gives us insight into the broad trends necessary to emulate the observations. Indeed we see a decrease retraction length, a decrease in loop bend and most notably an increase in apex loop top temperatures and densities as time advances. This strongly suggests a mechanism whereby the initial flaring drives an enhancement in temperature and density for later loops.

1 Introduction

Solar flares are highly energetic events which result in hard x-ray emission. In order to drive such energy release there needs to be a mechanism whereby the free magnetic energy can be accessed. [Parker, 1957] and Sweet [1958] laid the foundations for such a mechanism as they proposed magnetic reconnection. A current sheet brings together field lines of different orientation and then through the non-ideal behaviour within a diffusion region, the field lines can break and reconnect. [Petschek, 1964] advanced these ideas further by introducing slow mode shocks to the reconnection outflows. These facilitate an increased reconnection rate and a heating of the plasma consistent with that required by flares. This model has been investigated and fine tuned extensively since. However the fundamental concept remains the same. A change in topology results in a new field configuration which is then able to accelerate flows and heat the plasma.

In this report we will be analysing the validity of the Post Reconnection Evolution of a Thin Flux Tube (PREFT) model as developed and discussed by [Longcope et al., 2009], [Guidoni and Longcope, 2010] and [Longcope et al., 2016]. Initialising a bent tube after an assumed patchy reconnection event, the TFT is numerically evolved in accordance with the energy and momentum equations. It has been found that the magnetic energy is thermalized via gas dynamic shocks (GDS) which manifest as a density spike at the loop top.

In order to test this model we need some way to compare it with reality. Indeed, our understanding of flare behaviour is best probed through spectral observations of these events and thus a physically consistent flare model should be able to simulate such spectra. [Longcope et al., 2016] investigated this by synthesising light curves and comparing with the February 26$^{\text{th}}$ 2004 X-class flare. This particular event exhibited negligible non-thermal features and hence the theory of thermal free-free interactions was used to construct a synthetic spectral response function for the PREFT loop. By convoluting the light curves for a single retracting loop with the observed flux transfer rate, the net spectrum can be generated and compared with RHESSI observations. The PREFT run initialisation parameters were carefully chosen to find a strong fit at a particular time during the impulsive phase of the flare. This proved successful as a good fit was achieved. However, at earlier and later times the synthesised spectra deviated noticeably from the soft and hard extremes of RHESSI. Furthermore the synthesised GOES channels provided a somewhat unsatisfactory fit through time.

This is not entirely surprising considering the synthetic light curve only incorporates the convolution of a single retracting loop type. Indeed

over the course of a flare there is a range of loops all exhibiting different initialisation parameters. In order to better capture this temporal variation, a novel new multi-convolution technique has been developed whereby different loop types are 'triggered' at different times. This is enacted by distributing the flux transfer rate between the different tubes such that the net transfer rate is conserved but each loop dominates the share of flux at different times.

We will show that this technique reduces comparison errors with RHESSI observations and also provides a markedly improved GOES fit. Furthermore, the parameter trends used give us insight into the temporal evolution of loop properties. Most notably we discover the need for an increasing initial loop top temperature and density as time progresses. Such enhancements are able to explain the softening of the spectrum with time and lend support to the existence of some driving mechanism.

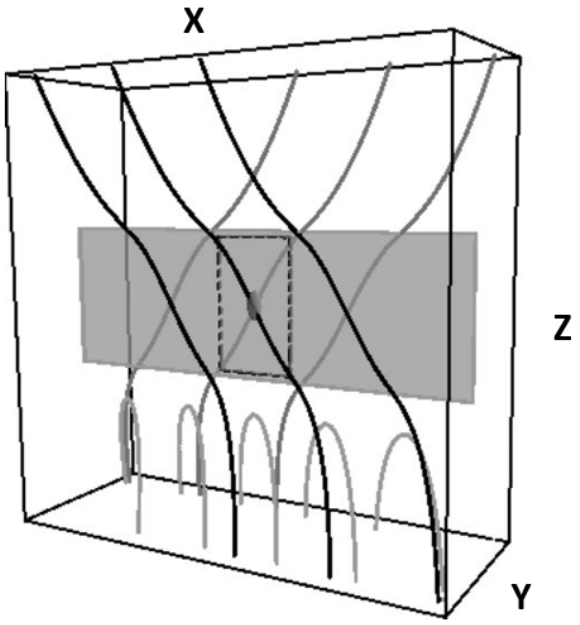

Figure 1: The field lines meet at the grey current sheet above the post flare arcade. Patchy reconnection occurs within the diffusion region indicated by the dashed box.

2 PREFT Background

2.1 Flux Tube Geometry

The PREFT tube is formed during a reconnection event between two uniform magnetic field regimes brought together at a current sheet. The geometry of the pre reconnection state is shown from the side in the Figure 1 adapted from [Guidoni and Longcope, 2010] and in Figure 2 from the x-y and x-z plane respectively. Note that the presence of a 'guide field' in the x direction parallel to the current sheet results in a bent triangular set-up characterised by the angle $\Delta\theta$. By parametrising along the length of this bent TFT we are able to capture the broad 2D physical behaviour using a 1D model, thus allowing for increased spatial resolution.

2.2 Initialising Tube Parameters

The geometry of this model leaves several free parameters to be determined - each affecting the subsequent retraction dynamics and synthesised spectra. Some of these can be constrained observationally as performed by [Longcope et al., 2016] with regards to the Feb 26^{th} 2004 event. Linear force free field (LFFF) extrapolations from the MDI magnetogram measurements provide a selection of analytical field lines which closely resemble those post-retraction cooled loops observed in TRACE 171$\mathring{A}$ images. This educates us on our choice of final loop length L_f and magnetic field strength B which is taken to be 200G throughout this study. The initial tube properties are less well constrained and are open to trial and error variation. The simplest initialisation is through use of the RTV scaling relationship developed by [Rosner et al., 1978]. Here they show that apex temperature is directly proportional to the pressure p and initial loop length L_0:

$$T_{\mathsf{apex}} \propto (pL_0)^{1/3} \tag{1}$$

Hence by choosing T_{apex} and L_0 we are able to set both the loop pressure and density (as related through the equation of state). Finally the tube is bent into the triangular configuration specified by $\Delta\theta$ and we are ready to examine the retraction dynamics.

2.3 TFT Equations

Having defined the geometry of the problem and constrained/guessed the initialisation parameters, the flux tube can now be evolved in accordance with the TFT equations as described by Longcope et al. [2016] and outlined below.

$$\begin{aligned}\rho\frac{d\mathbf{v}}{dt} = &\left(\frac{\mathbf{B^2}}{4\pi} - p\right)\frac{\partial\hat{\mathbf{l}}}{\partial l} - \hat{\mathbf{l}}\frac{\partial p}{\partial l} \\ &+ \frac{4}{3}\frac{\partial}{\partial l}\left[\hat{\mathbf{l}}\mu\left(\hat{\mathbf{l}}\cdot\frac{\partial\mathbf{v}}{\partial l}\right)\right] + \rho\mathbf{g}\end{aligned} \tag{2}$$

This is the momentum equation and simply encapsulates $\mathbf{F} = m\mathbf{a}$. The left hand side corresponds to the acceleration of a plasma element whilst the right hand side sums the contributions

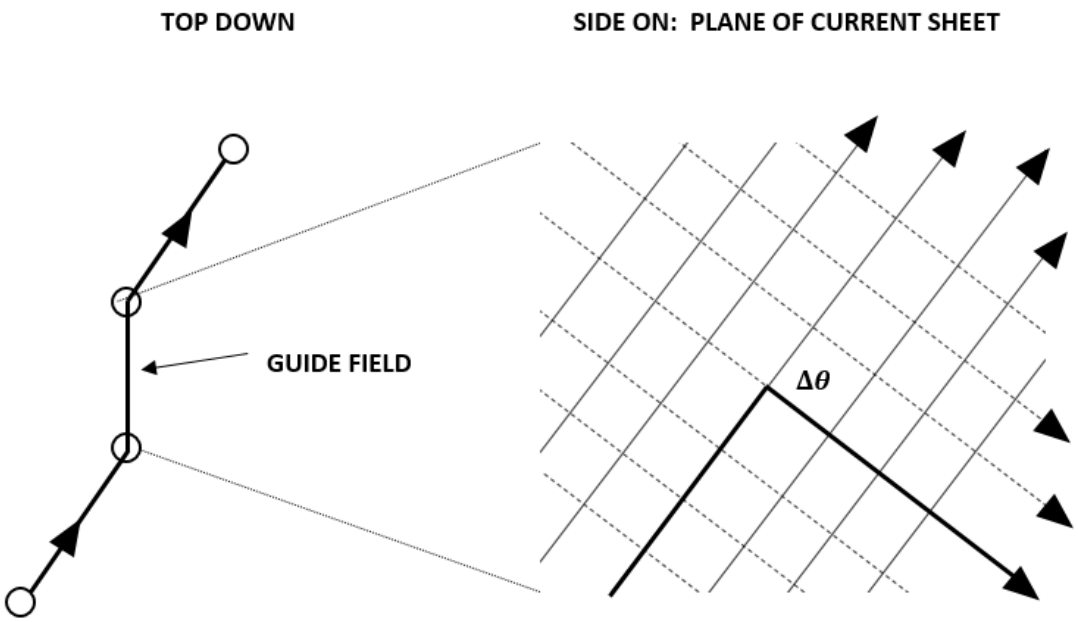

Figure 2: The left diagram is provides a top down (x-y plane) view of the flux tube at the moment of reconnection. This overall loop is then approximated as the triangular tube in the x-z plane as shown on the right.

from each force present. The first term is the combination of magnetic and plasma tension. The second term is the plasma pressure gradient along the tube. The third term is the viscosity which is essential for thermalizing the released magnetic energy. The final term is the gravitational acceleration which is negligible in the corona. The temperature is then evolved through the energy equation as follows.

$$\begin{aligned} c_v \rho \frac{dT}{dt} = &- p\hat{\mathbf{l}} \cdot \frac{\partial \mathbf{v}}{\partial l} + \frac{\partial}{\partial l}\left(\kappa \frac{\partial T}{\partial l}\right) - n_e^2 \Lambda(T) \\ &+ \frac{4}{3}\mu \left(\hat{\mathbf{l}} \cdot \frac{\partial \mathbf{v}}{\partial l}\right)^2 + h \end{aligned} \tag{3}$$

Once again the right hand side terms have clear physical meanings. The first term is work done. The second is thermal conduction. The third accounts for optically thin radiative losses and the fourth is the energetic dissipation due to viscosity - complementing the term in the momentum equation above. The final term is an ad hoc coronal heating function which is input to establish the initial equilibrium of the tube but has no significant impact on the subsequent evolution.

2.4 Dynamical Evolution

Now that the key aspects of the model have been summarised let us examine a typical TFT retraction and identify the main physical features. Figure 3 illustrates an example PREFT run during the retraction phase. This is initialised with $L_0 =$ 79Mm, $L_{\mathsf{fin}} =$ 57Mm, $T_{\mathsf{apex}} =$ 8.5 MK and $\Delta\theta =$ 110°.

The magnetic tension term causes the triangular peak to accelerate downwards and resolve itself into two rotational discontinuities (RDs) which propagate at approximately the Alfvén speed, V_A down the legs. This causes both a z velocity component, which translates the horizontal section of the TFT downwards, and also an inwards x velocity component. The inward plasma flow results in a loop-top collision causing the density to spike in a GDS. Continued inwards flow is able to maintain this shock for a considerable period. It is here that viscosity thermalizes the horizontal kinetic energy component and we see a corresponding temperature peak. This then spreads down along the loop towards the foot points, ahead of the RD's, as a thermal conduction front. This drives chromospheric evaporation which causes another source of inwards plasma flow.

After the loop has retracted to the specified final length it is artificially straitened to signify the end state in the post flare arcade configuration. The loop top source persists for a considerable time beyond this however as the GDS is stabilised by upwards evaporation. Competing evaporative flows and GDS dissipation flows repeatedly collide and bounce back and forth between the loop top and chromosphere. Eventually the dissipative effects win

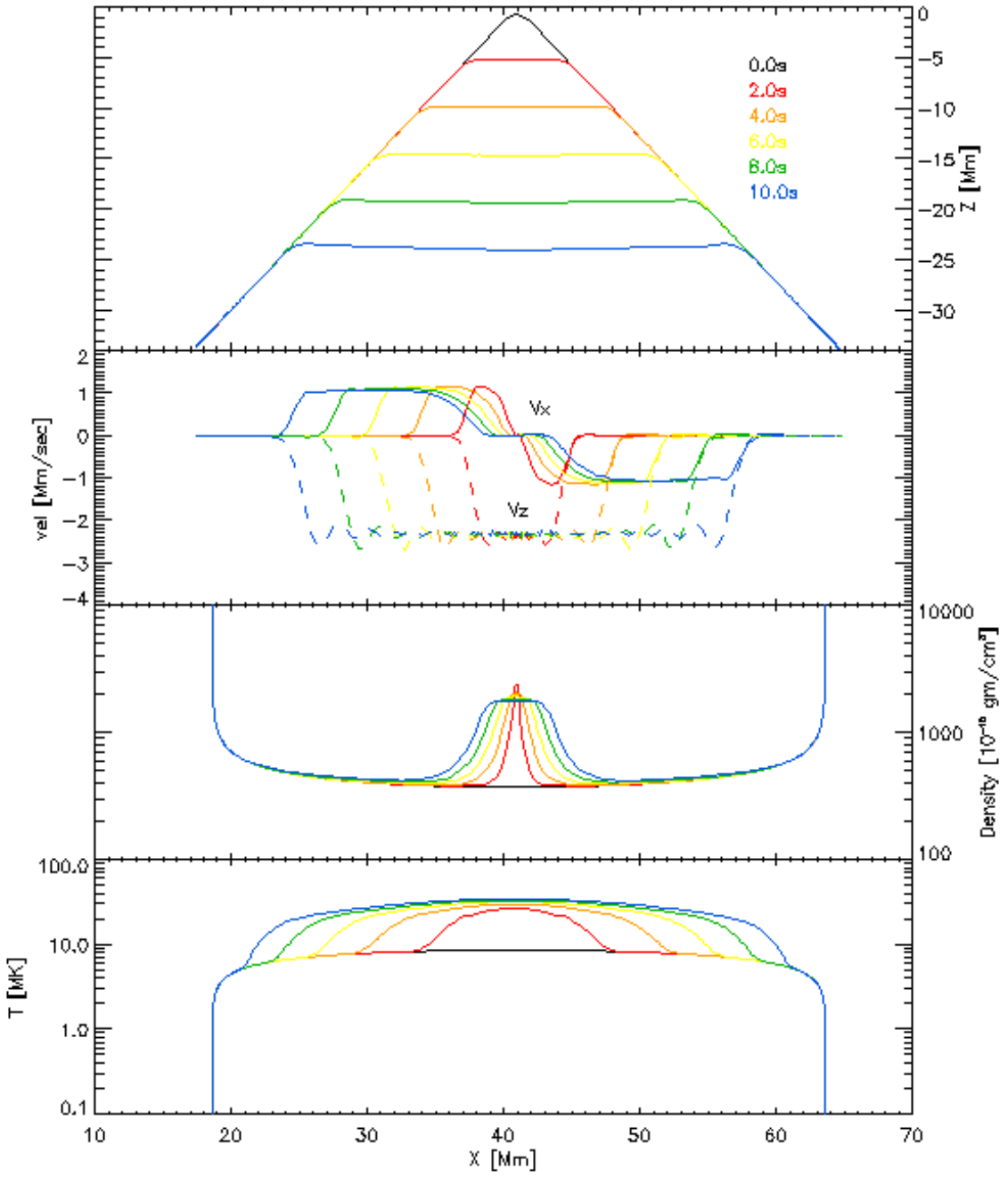

Figure 3: Here we see the evolution of an example PREFT run during the retraction phase at 2 second time intervals.

and smooth out the central density peak whilst the plasma velocity is reduced by viscosity. The temperature profile smooths and then slowly reduces as it cools radiatively towards the final RTV equilibrium state.

It should be emphasised again that it is the conversion of stored magnetic free energy into horizontal flow which is driving the flare. This is formally outlined by [Longcope et al., 2016] as they show that the shortening of the TFT is coupled with an energy release per unit flux at a rate:

$$\dot{W_M} = \frac{B}{4\pi}\frac{dL}{dt} = \frac{B}{4\pi} 4 v_a \sin^2(\Delta\theta/4) \qquad (4)$$

By extracting the horizontal fraction of the resulting kinetic energy they show that the flare energy flux associated with each leg is given by:

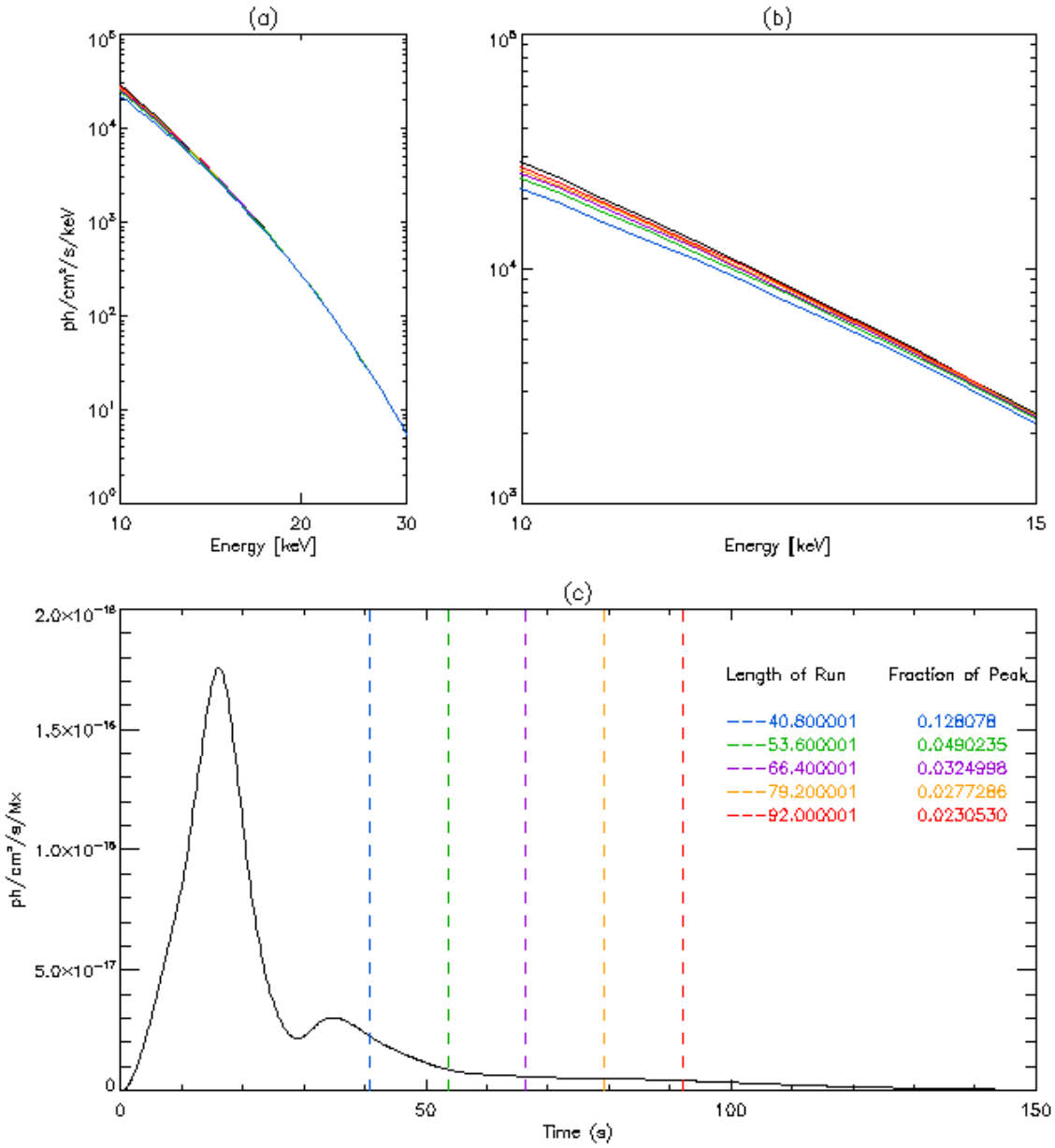

Figure 4: (a) Shows the synthesised spectra for the different lengths of PREFT run as indicated by the different colours. (b) Shows a zoomed in region where there is notable spectral variation. (c) Shows the light curve integrated over the energy interval 10-30keV. The dashed coloured lines indicate the different length runs used to synthesise spectra.

$$F_{fl} \simeq \frac{1}{2} B \dot{W}_M \sin^2(\Delta\theta/4) \tag{5}$$

Note that this depends on both the angle of the tube and the alfvén speed which is inversely related to the root of density. Hence our tube initialisation will directly affect the rate of energy deposition. Furthermore the total length retracted through will affect the net energy release. Thus we immediately see the importance of our parameter choices in the energetic behaviour of the TFT.

3 Spectral Synthesis

3.1 Synthesis Procedure

The next step requires us to perform spectral synthesis. This is initially done for a single retracting loop using the procedure developed by [Longcope et al., 2016]. The theory of free-free interactions is well understood and allows us to construct the spectral response function $R[T(l,t)]$, for a particular energy band. Then integrating over the loop length a light curve for this band is found:

$$I_0(t) = \int n_e^2(l,t) R[T(l,t)] \frac{dl}{B} \tag{6}$$

This gives the photon rate per unit flux so should be convolved with the flux transfer rate $\dot{\phi}(t)$ to attain the net signal:

$$I(t) = \int^t (t-s)\dot{\phi}(s) ds \tag{7}$$

The flux transfer rate used in this report is that obtained by [Longcope et al., 2016]. They solved the inverse problem of finding the $\dot{\phi}(t)$ which matches the simulated emission for a particular energy interval with the same RHESSI observed emission band. This rate can then be used to synthesise all other bands.

3.2 Length of PREFT Run Required

In order to synthesise a spectra which accurately reflects the infinite time limit of the PREFT run we must ensure that the simulation is continued to a suitable number of iterations - thus ensuring that we don't miss out on important spectral emission in the tail. We have incorporated a simple check to enforce this. By comparing the synthesised spectra using different different temporal lengths of the same PREFT run we can see at what time the spectra stops changing noticeably. Figure 4 shows that in all cases chosen there is only an appreciable variation in the soft energy regime. This makes sense as the PREFT runs used are all cut off in the emission tail where the loop has cooled and the hard emission has dropped off. By the time the light curve has plateaued between the green and purple marker we see the synthesised spectra exhibits little meaningful change. Hence we incorporate the light curve in a simple check before any analysis and observational comparisons are performed. Indeed we posit the criteria that the 10-30keV light curve must have dropped to below 0.04 of its peak value before proceeding further.

3.3 Comparison with RHESSI

We are now ready to compare the synthesised spectra with RHESSI observed spectra, placing particular emphasis in achieving a good fit between the energy range 10-30keV. Below this, emission effects are present which are not modelled by the thermal bremsstrahlung synthesis procedure. Above this range, the count rates observed are small and dominated by noise.

In order to have a quantitative comparison between the synthetic and observed spectra we introduce an error measure termed the Logarithmic Root Mean Square Deviation (LRMSD):

$$LRMSD = \frac{\sqrt{(\sum \log Y_{RHi} - \log Y_{PREFTi})^2}}{N} \tag{8}$$

The RHESSI and PREFT data points are interpolated onto a common grid giving us Y_{RHi} and Y_{PRi} respectively. We define a good fit as one which minimises the factor differences between the two curves rather than the absolute differences. This ensures that the hard x-ray regime is treated with the same significance as the soft despite the absolute photon count being less. Such factor differences correspond to normal visual differences when plotted on a logarithmic scale hence we employ the logarithmic difference in the root mean square calculation.

Having formalised the comparison we are now able to produce the spectral plots for the example run discussed previously for three different times during the flare. The results are shown in Figure 5. Here we see that a single loop type can achieve a good fit at a particular time but will deviate from RHESSI at other times. Indeed the example loop provides a good fit at the intermediate time of 02:00:50 but is too hard at later times and too soft at earlier times. This reiterates the findings of [Longcope et al., 2016] as shown below in Figure 6.

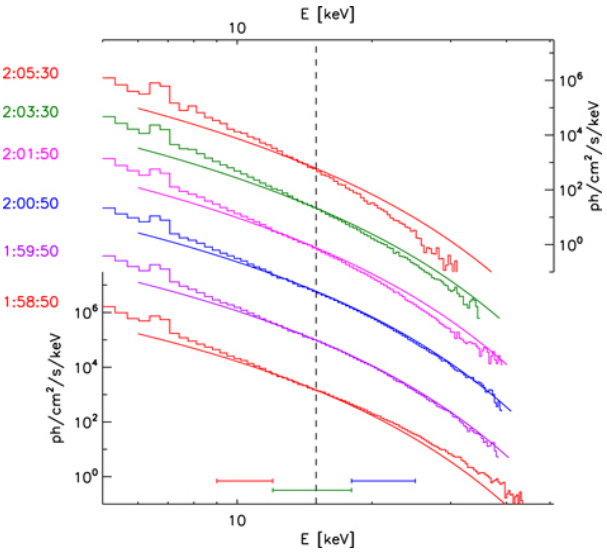

Figure 6: Results taken from [Longcope et al., 2016] illustrates the effective fit at a particular time and deviations at other times. Note the different time plots have been vertically displaced for easier comparison.

This motivates the fundamental aim of this study which seeks to find loops which offer an improved fit at other times of the flare. Considering the LRMSD value of 0.06 found for the time 02:00:50 in the example run, we seek PREFT parameters which allow us to achieve a similarly small error.

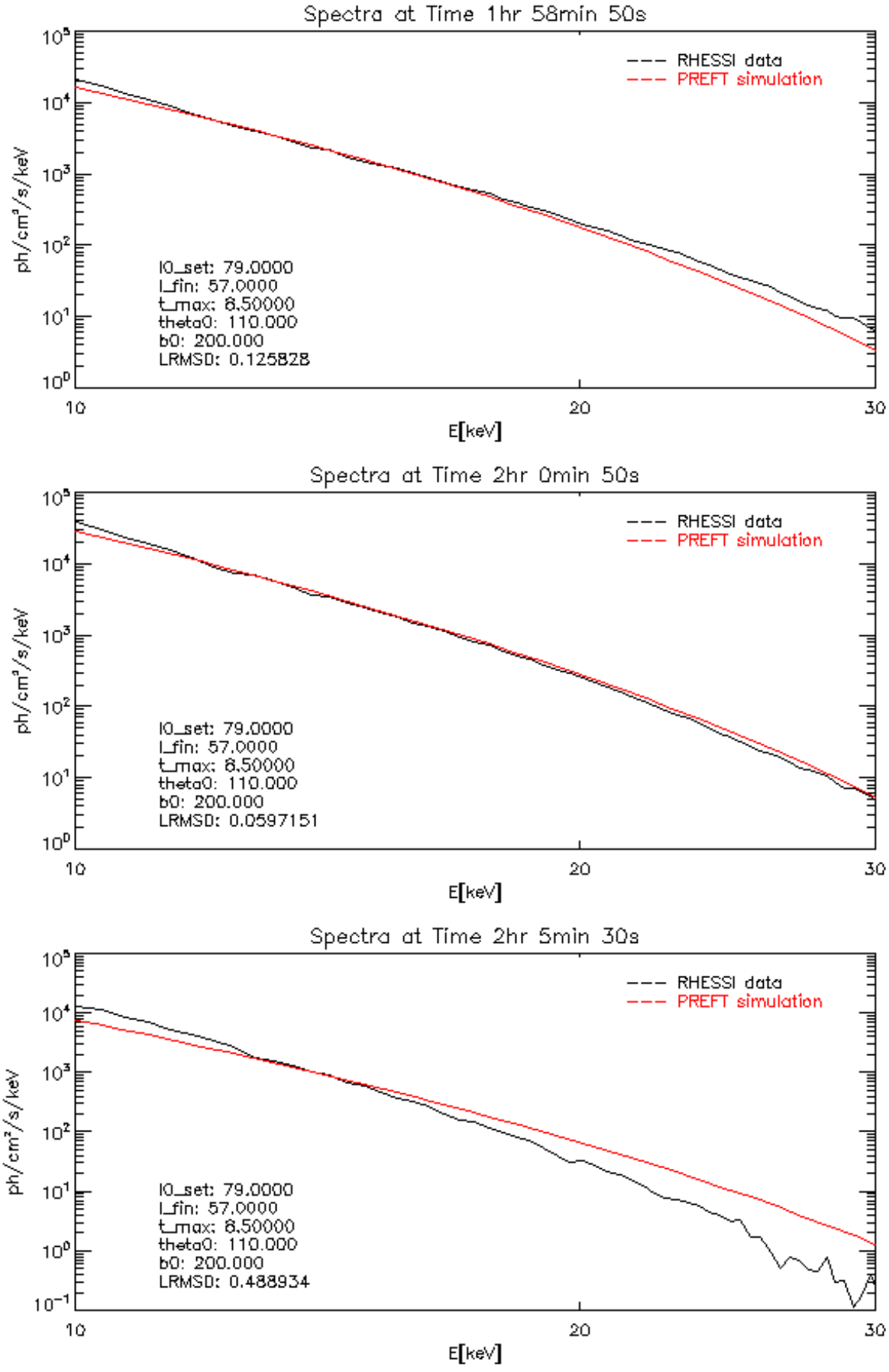

Figure 5: 01:58:50 - This earlier time shows a synthetic spectra which is too soft. 02:00:50 - This intermediate time shows a good fit across all energies. 02:05:30 - This later time shows a clear deviation as the synthesised spectra is too hard.

4 Parameter Variation

In order to find appropriate runs for different times we must first develop a working intuition which allows us to predict how varying a parameter will effect the resulting spectra. This is initially investigated by systematically changing a given parameter whilst keeping the others constant and then examining the spectral changes for a given time - taken to be 02:00:50. The extremum limits of such variations are shown in figure 7 overleaf with the corresponding parameter choices tabulated below.

Table 1: Apex Temperature Variation

Fixed			**Varied**	
L_0 (Mm)	L_{fin} (Mm)	$\Delta\theta$ °	T_{apex} (MK)	
67.0	45.0	110	6.5	11.0

Table 2: Length Variation

Fixed		**Varied**			
T_{apex} (MK)	$\Delta\theta$ °	L_0 (Mm)		L_{fin} (Mm)	
7.5	110	60.0	89.0	40.0	60.0

Table 3: Angle Variation

Fixed			**Varied**	
L_0 (Mm)	L_{fin} (Mm)	T_{apex} (MK)	$\Delta\theta$ °	
67.0	45.0	7.5	105	115

4.1 Temperature Variation

Here we see that as the initial apex temperature is increased the spectra actually becomes softer - performing a 'pivot' motion with increased emission at low energies and decreased emission at high energies. At first thought, an increased T_{apex} producing a softer spectra might seem surprising. However the behaviour has a clear physical explanation. Indeed we recall that apex temperature is intimately linked to the pressure via the RTV scaling relationship described in equation 1. Applying the equation of state we understand $T_{\text{apex}} \propto \rho^{1/2}$. Thus since the Alfvén speed is given by

$$V_A = \frac{B}{\sqrt{\mu_0 \rho}} \tag{9}$$

we see that as T_{apex} increases and ρ increases then V_A actually decreases. Hence the inward velocity flows accelerated by the RD bends are reduced and the corresponding GDS collision is less violent. Thus the larger the initialisation temperature, the smaller the maximal apex temperature and hence the softer spectrum. Such a description is supported by plotting the apex temperature variation against time for all the temperature trial runs examined as shown in figure 8.

Here wee see the typical temperature profile is the same shape but for smaller initialisation T_{apex} it is stretched upwards to higher peak temperatures and squashed temporally indicating the faster retraction. This reflects the increased Alfvén speed which dictates the characteristic time scales in which the system evolves.

4.2 Length Variation

Here we have scaled up both the initial and final lengths such that the overall length retracted through increases. We observe increased emission across the whole spectra with the largest logarithmic increase at high energies. As the flux tube retracts through a larger length more magnetic free energy is liberated so an increased emission should be expected. Furthermore, the enhanced effect at higher energies again can be traced back to the RTV scaling. As L_0 increases then ρ decreases to satisfy the equilibrium. Hence the Alfvén speed increases and the inwards flows are faster - resulting in a harder x-ray source at the loop top.

4.3 Angle Variation

As the angle is increased the tube becomes more bent and we see the spectra responds by pivoting upwards at the high energies. As $\Delta\theta$ increases there is faster and more efficient conversion of the magnetic energy into horizontal kinetic energy in accordance with equations 4 and 5. The inwards flows are larger and and hence the loop top temperatures can rise higher. This once again generates a harder spectral response.

4.4 Scaling Law

These effects can be incorporated into a single scaling law which link all the initialisation parameters to the maximal apex temperature achieved - hence theoretically justifying the hardening or softening of the spectra. Combining equation 5 with the definition of the Alfvén speed we see the combined flare energy flux through both legs must be:

$$F_{fl} = \frac{B^2}{\pi} \sin(\Delta\theta/4) \frac{B}{\sqrt{\mu_0 \rho}} \tag{10}$$

Assuming an approximately steady state energy density within the loop top then the energy flux must be balanced by thermal conduction to the foot points:

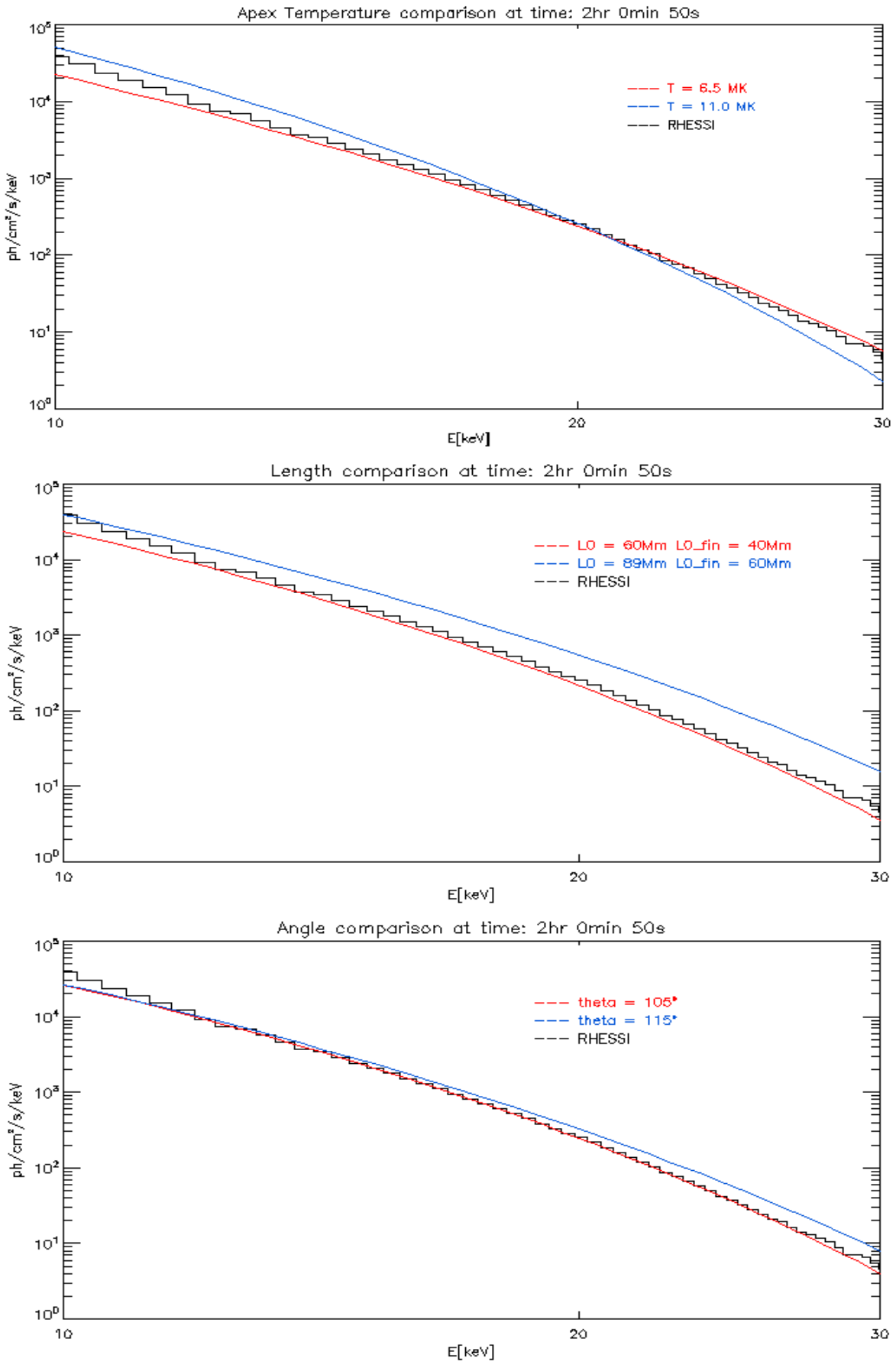

Figure 7: This illustrates the effect of changing a given initialisation parameter when the others are held fixed. Temperature: Shows a pivoting behaviour. Length: Shows a vertical translation. Angle shows a slight pivoting behaviour significant at the high energies.

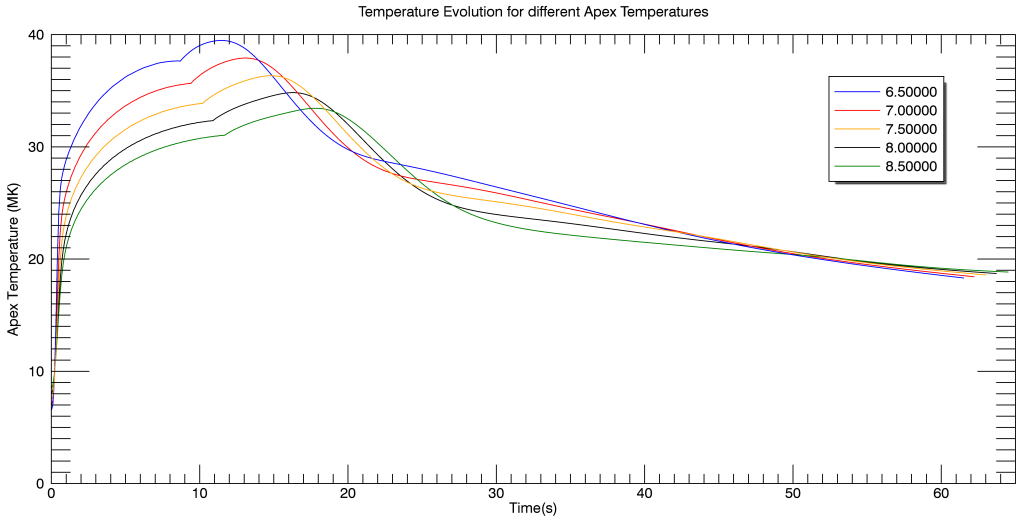

Figure 8: Apex temperature evolution for a variety of initialisation temperatures indicated by different colours.

$$\frac{F_{fl}}{L_f} = \frac{\partial}{\partial l}\left(\kappa \frac{\partial T}{\partial l}\right) \tag{11}$$

Inserting characteristic quantities and using the classical Spitzer-Härm form for the conduction coefficient κ we find:

$$\frac{B^3}{\pi L_f \sqrt{\mu_0 \rho}} \sin\left(\Delta\theta/4\right)^4 = \frac{\kappa_0 T^{7/2}}{L_f^2} \tag{12}$$

Now inserting the RTV relationship $T_{apex}^2 = \rho \mathrm{L}_0$, cancelling terms, rearranging and dropping constants we find the scaling law:

$$T_{\mathsf{max}} \propto L_f^{2/7} L_0^{1/7} B^{6/7} T_{apex}^{-2/7} \sin(\Delta\theta/4)^{8/7} \tag{13}$$

This is a powerful relationship which corroborates our previous physical reasoning. Indeed it suggests that increasing length scales result in increased maximal temperatures, as does an increasing angle. Meanwhile as the initial temperature is boosted, the negative exponent ensures that the maximal apex temperature decreases. Exploiting this improved understanding of our parameter space we are now able to proceed with the task of finding PREFT runs which match the RHESSI observations at a set of different times. By using the basis of pivoting and translational shifts related to parameter variations, we can now perform educated trial and error runs until effective fits are found.

5 Multi Convolution

5.1 Effective Fits

We have been able to find parameter choices which provide an effective fit to RHESSI observations at multiple times throughout the impulsive phase of the flare. These are detailed in table 4 and plotted in figure 9.

We have identified 7 times with an suitably minimised error. The slight increase in the LRMSD for 6900s represents the short term presence of non-

Table 4: Multi Convolution Run Parameters for different times

Time (s)	L_0 (Mm)	L_f (Mm)	δL (Mm)	T_{apex} (Mk)	$\Delta\theta$ (°)	LRMSD
6900	110	80	30	7.0	115	0.1487
7130	74	50	24	7.5	110	0.0548
7190	67	45	22	8.0	110	0.0524
7250	67	45	22	7.5	110	0.0649
7310	65	45	20	10.5	109	0.0699
7410	65	45	20	10.5	109	0.0745
7550	67	47	20	11.5	102	0.1018

Figure 9: Apex temperature evolution for a variety of initialisation temperatures indicated by different colours.

(a)

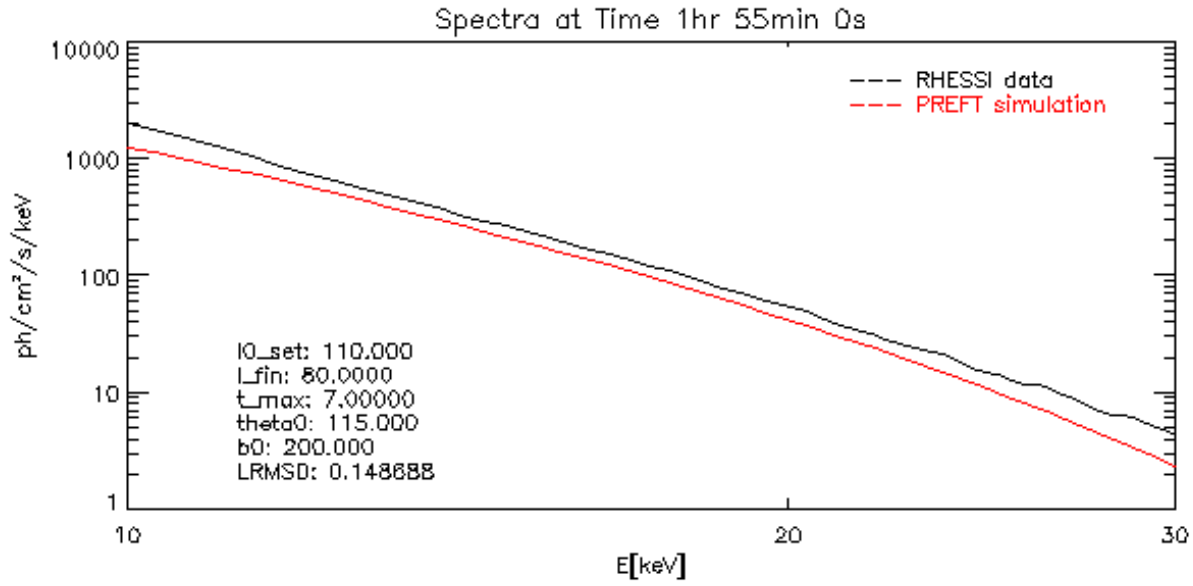

(b)

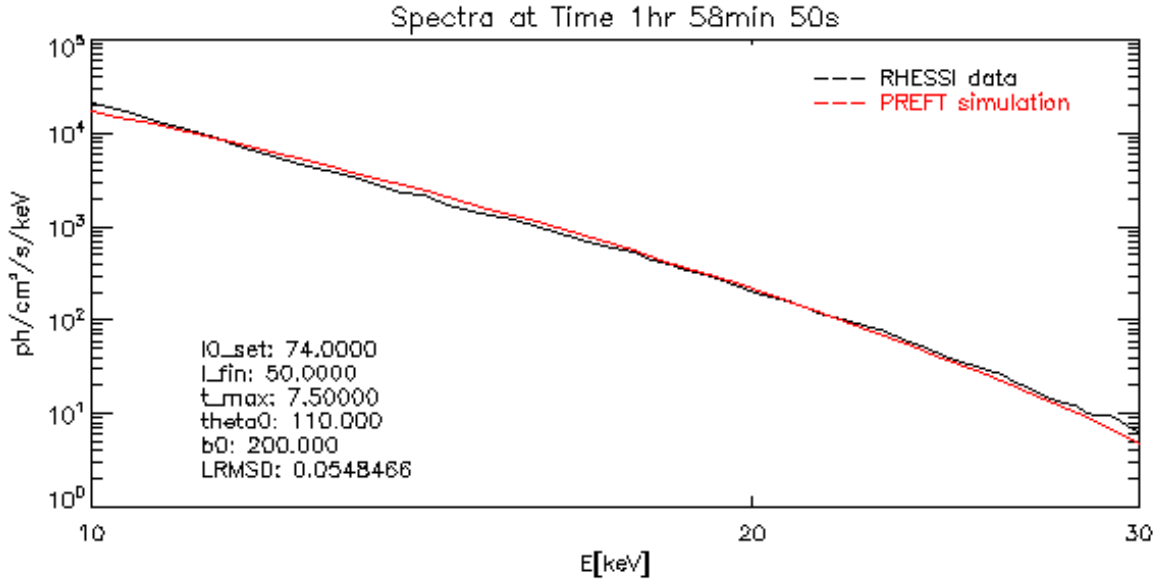

(c)

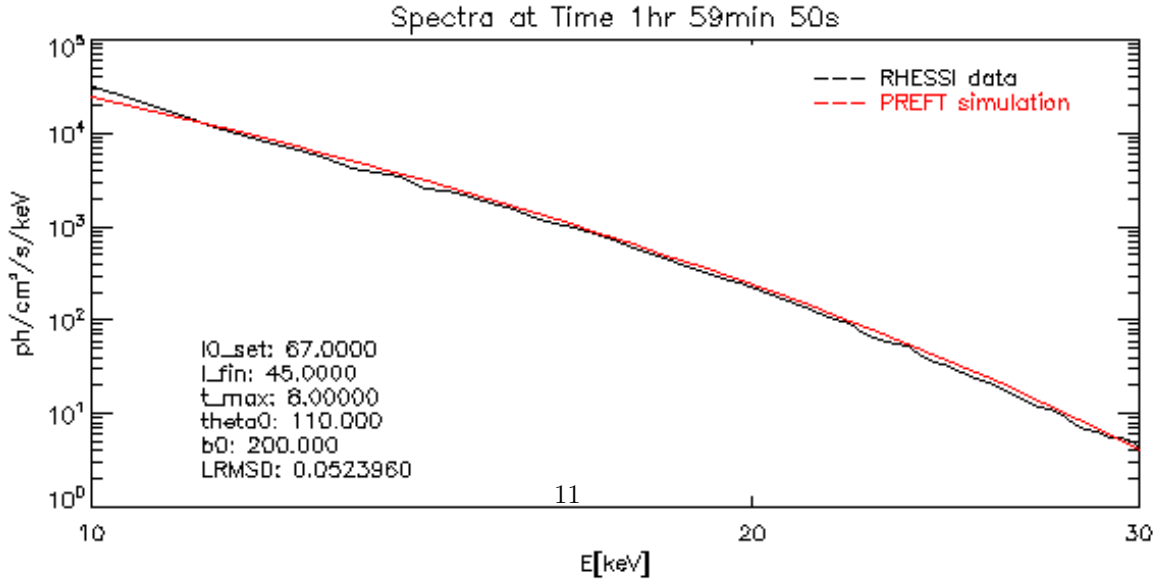

(d)

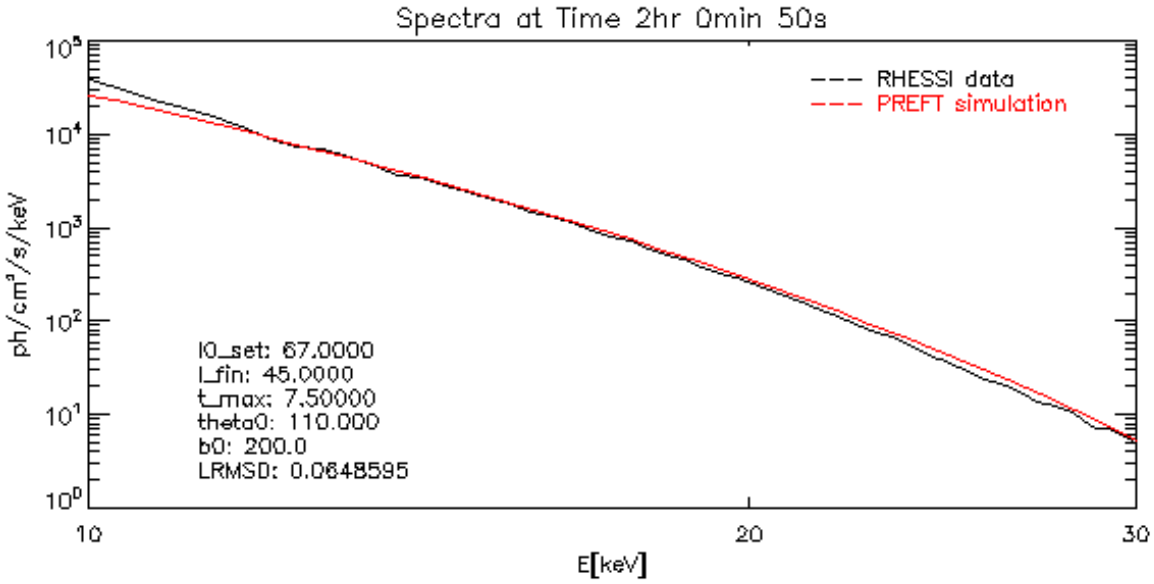
Spectra at Time 2hr 0min 50s
RHESSI data
PREFT simulation
I0_set: 67.0000
I_fin: 45.0000
t_max: 7.50000
theta0: 110.000
b0: 200.0
LRMSD: 0.0648595
ph/cm²/s/keV
E[keV]

(e)

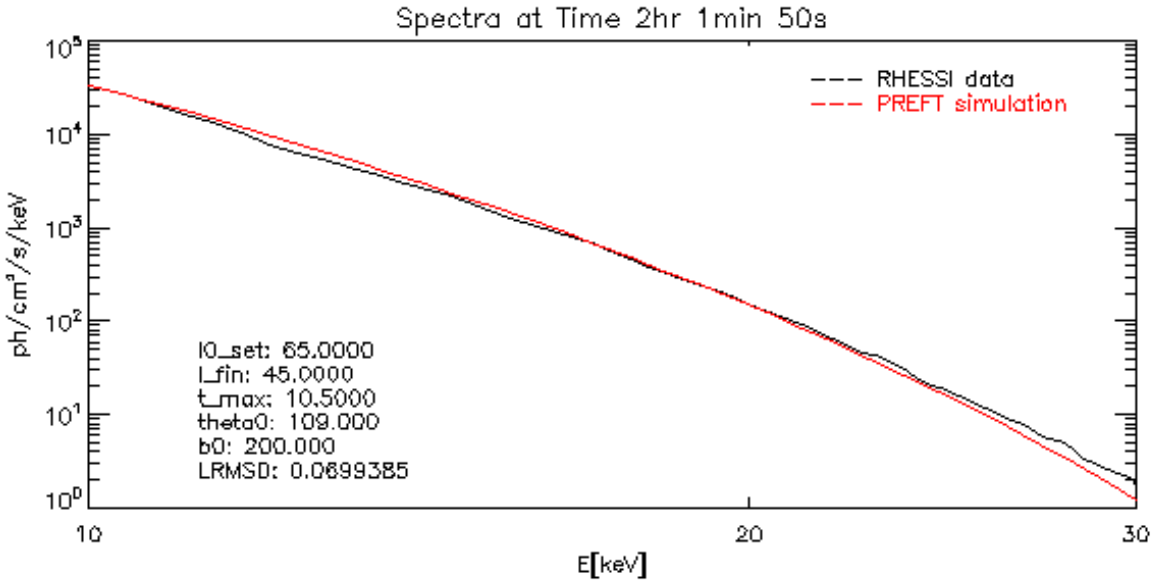
Spectra at Time 2hr 1min 50s
RHESSI data
PREFT simulation
I0_set: 65.0000
I_fin: 45.0000
t_max: 10.5000
theta0: 109.000
b0: 200.000
LRMSD: 0.0699385
ph/cm²/s/keV
E[keV]

(f)

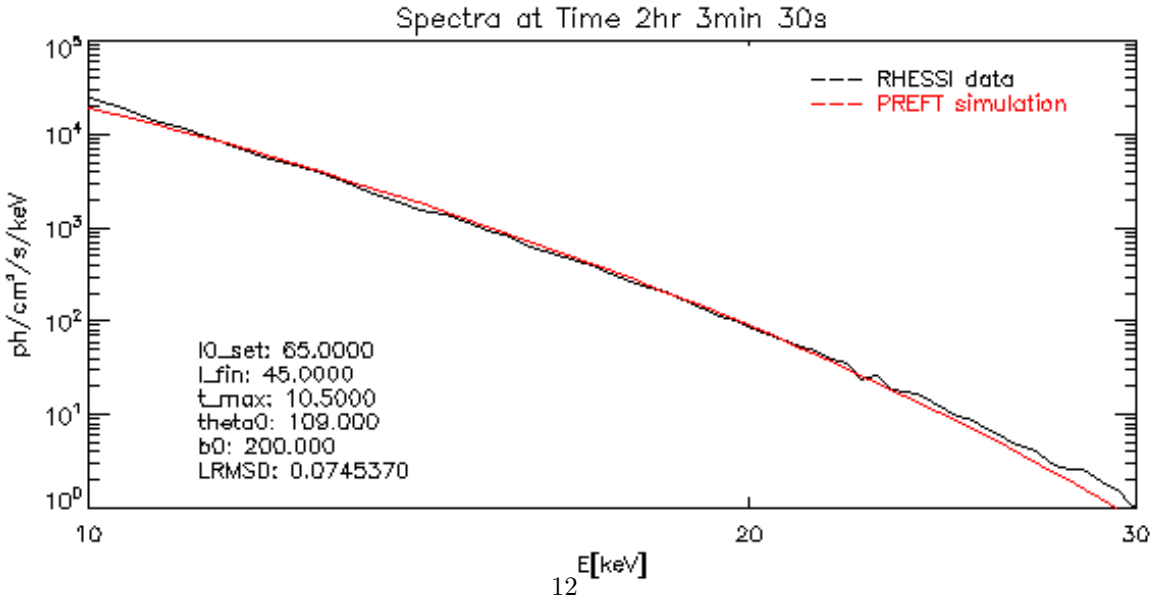
Spectra at Time 2hr 3min 30s
RHESSI data
PREFT simulation
I0_set: 65.0000
I_fin: 45.0000
t_max: 10.5000
theta0: 109.000
b0: 200.000
LRMSD: 0.0745370
ph/cm²/s/keV
E[keV]

(g)

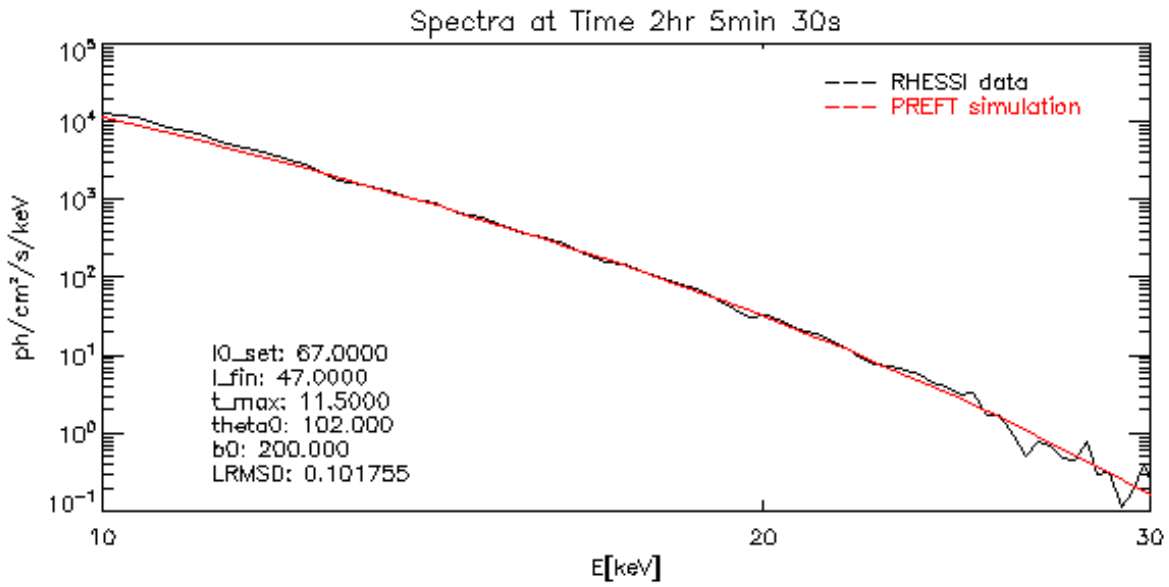

thermal effects which are not incorporated within the model. Indeed, at the onset of the impulsive phase RHESSI reports a power law spectrum indicative of such non thermal activity. Also at 7550s we see the larger error measure is simply an artefact of the increased noise at the high energies of the RHESSI spectra.

Note that each plot is still the result of a single loop convolution method examined at the particular time which corresponds to a good fit. These can now be carried forward and incorporated into the multi convolution method outlined in the following section.

6 Multi Convolution Method

6.1 Flux Transfer Distribution

The multi convolution method is a novel extension of the original convolution technique whereby the original flux transfer rate $\dot{\phi}(t)$ is now distributed between the different loop types - thus aligning itself with the physical reality that a host of loops are present throughout the course of a flare.

This distribution is designed such that the flux transfer share corresponding to a given loop type is maximised at the time we identified that loop to provide an effective fit. The light curve per unit flux obtained for a single loop type is then convolved with the associated flux rate share. This is repeated for all loops and the result summed to give us the net light curve for a given energy band. Repeating for each energy band allows us to construct the overall spectra. This process is summarised by equations 14 and 15.

$$I_{net}(t) = \sum_{i=1}^{7} \int I_i(t)\dot{\phi}_i(t-s)ds \tag{14}$$

$$\dot{\phi}(t) = \sum_{1}^{7} \dot{\phi}_i(t) \tag{15}$$

Employing this method we construct a temporally staggered set of seven triangular distributions such that at all times they sum to give one. We have constructed this so that at any time there is a maximum of two overlapping triangles indicating the mixing of two retracting loops. One is being 'switched off' as the other is 'switched on'. Multiplying these distributions by the net flux transfer gives us our seven flux shares $\dot{\phi}_i(t)$ as demonstrated in figure 10.

All the triangles except one have their peak aligned with the time with which the corresponding loop type was adjusted to fit. Note however that the orange component corresponding to the second loop (7130s fit) is peaked earlier at 6960s. Through examination of the later results we see that this helps reduce the mixing effects of the spectral contribution from the first loop which takes some time to die away. Indeed the spectral evolution is rather rapid at the onset of the impulsive phase before developing more smoothly at later times. This will be seen in the following results.

6.2 Initial Results

6.2.1 RHESSI Comparison

Performing the spectral synthesis on each loop/flux-rate pair and summing we get the final spectral

Figure 10: Flux Distribution Amongst 7 Loops Indicated by Different colours.

(a) Fraction of flux is distributed in triangular profile. As one loop is 'switched on' another is 'switched off'.

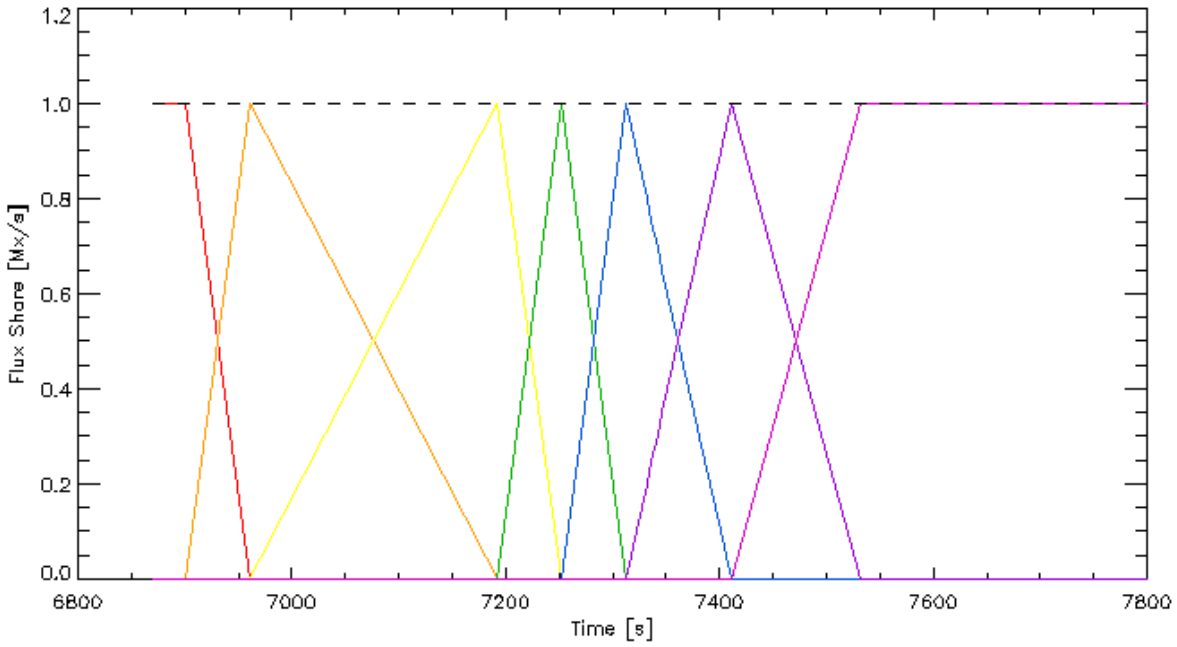

(b) Result of multiplying through by the flux share gives flux transfer corresponding to each loop in the different colours. The sum of which gives the total transfer rate in black.

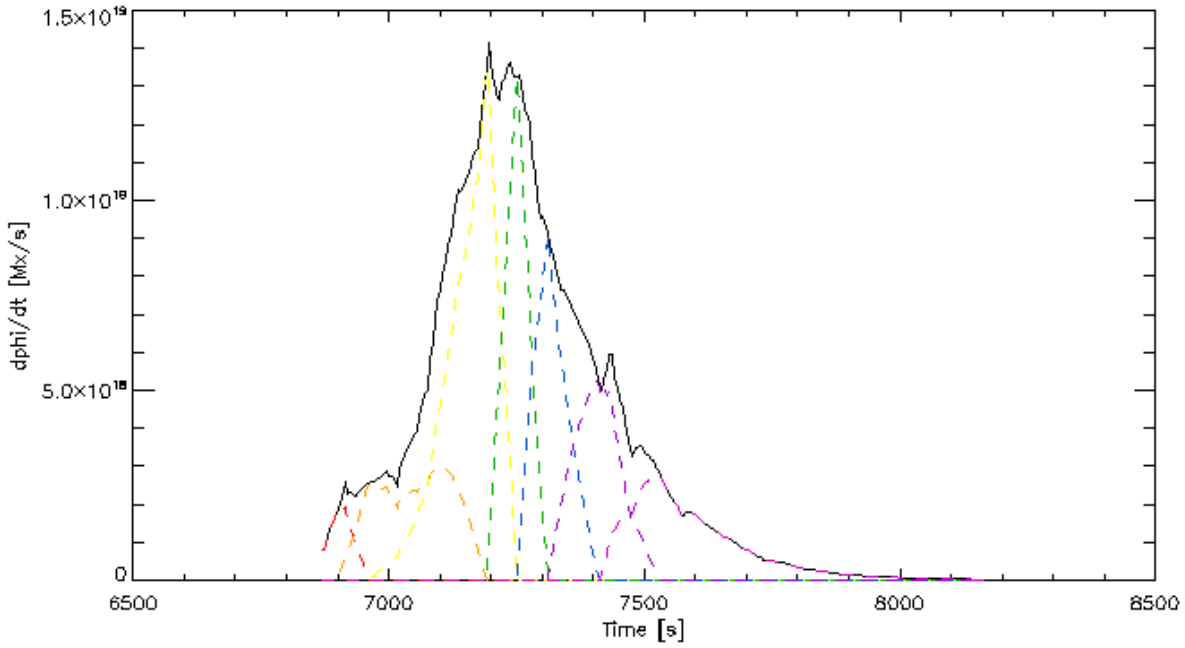

Figure 11: Multi Convolution Results (a) RHESSI LRMSD comparison with single loop (black) and multi loop (red) LRMSD. (b) GOES fit comparison with observed data

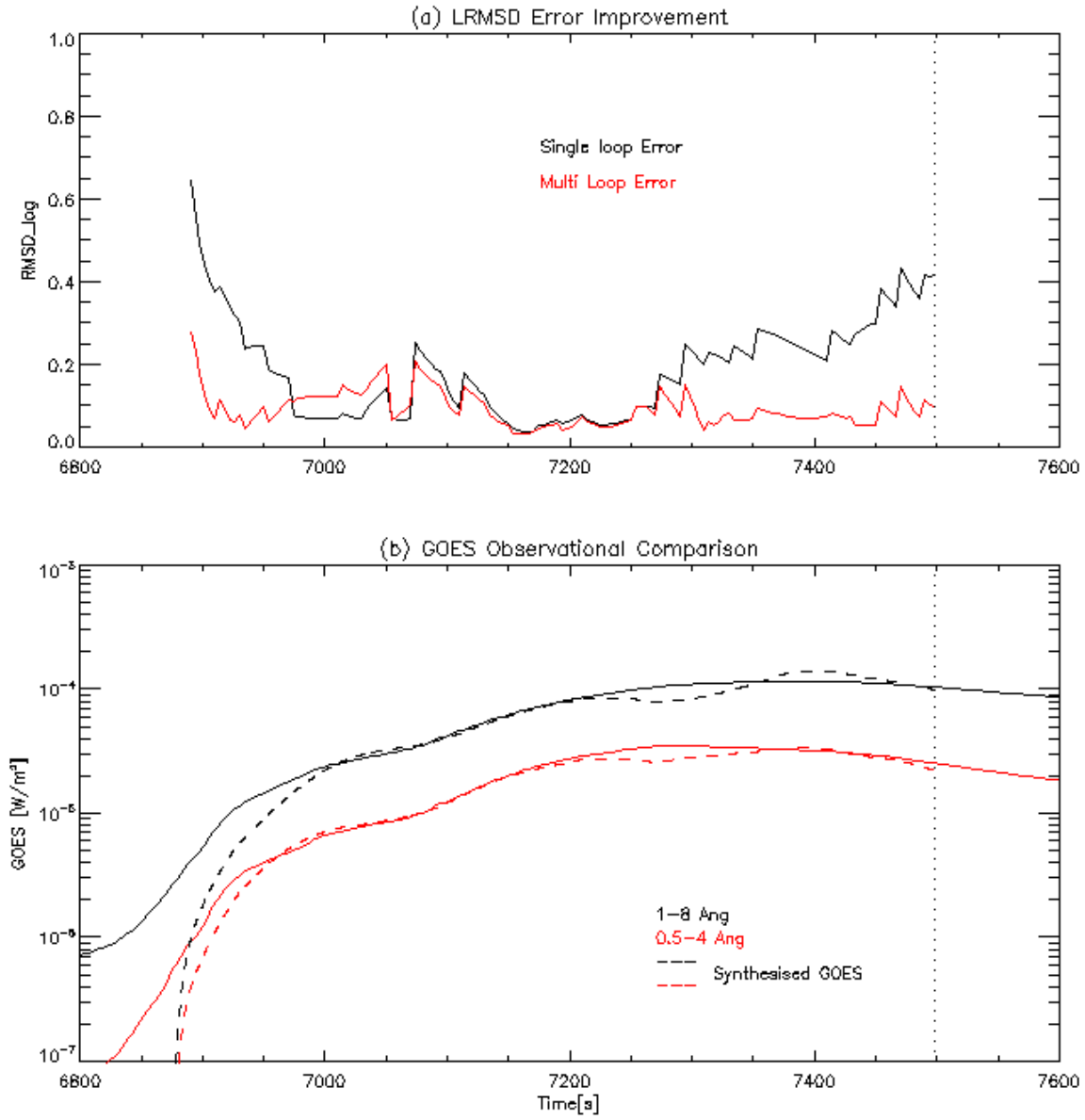

result over the impulsive phase of the flare. By comparing the LRMSD across all times for this multi convolution method with the error using only a single loop we can appreciate the improvement using this new technique. See figure 11.

The red multi convolution line consistently tracks an error path below that of the black line which only uses one loop - in particular the loop corresponding to the time 7250s. We note the drastic improvement at earlier and later times where the single loop method was previously lacking. This immediately acts as a proof-of-concept for the multi convolution method and suggests that incorporating further loops could improve the fitting further. Note that at times the red multi loop error line does rise briefly above the single loop line. This can be attributed to sudden changes in the flaring behaviour which is not accounted for by the smooth mixing of loops with gradual transitions between flux shares. Again adding more loops at these times could help counter this.

6.2.2 GOES Comparison

As an independent test of the new technique we are able to construct the synthesised GOES data in an analogous manner. The spectral response function used in equation 6 is now simply integrated over a larger bandpass corresponding to the two

Figure 12: Single loop GOES comparison deviates considerably at the later times from observation.

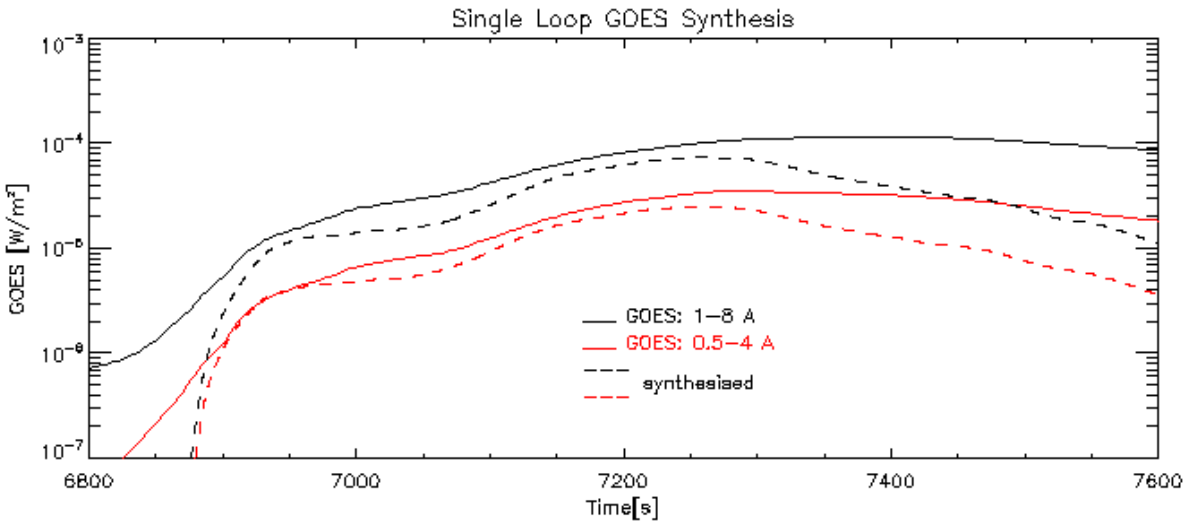

GOES channels: 1-8$\mathring{A}$ and 0.5-4$\mathring{A}$. This can then be compared with the observed GOES data. We see that in figure 11 (b) the synthesised channels provide a very good match with observation. The fantastic overlap is particularly encouraging considering no effort was hitherto made to fit GOES data. This demonstrates a vast improvement on the single loop technique explored by [Longcope et al., 2016] which found a less satisfying fit. Indeed if we compare with the synthetic GOES spectrum using only the 7250s single loop we see a large deviation at the later times especially. See figure 12.

Thus the effective RHESSI and GOES comparisons complement each other and lend support to the validity of this model and the parameters chosen.

7 Implications

With a successful demonstration of this method, there is much information to be extracted. Not only does the improved fit show that the PREFT model is capable of simulating observation to a high degree of accuracy, but it also provides us with a suggested average evolution of flare parameters, see figure 13. Over the course of fitting different times there was no effort to force particular patterns. Nonetheless we find three clear trends over the development of the flare - an increasing apex temperature, a decreasing change of length and a decreasing angle. The significance of these will be examined each in turn.

7.1 Temperature

The need to increase the initialisation temperature was the most prominent trend when finding effective fits for later times. Indeed, this seemed to be the only parameter capable of softening the spectra to the extent required. Progressing from 7.0 MK up to 11.5 MK, these represent controversially high temperatures for pre-retraction loops. However, this allows us to boost the loop top density through the RTV scaling and achieve the increased emission necessary to match the GOES data at later times. This implies the need for some mechanism which drives temperature and density enhancement within the current sheet as the flare progresses through the impulsive phase.

7.2 Angle

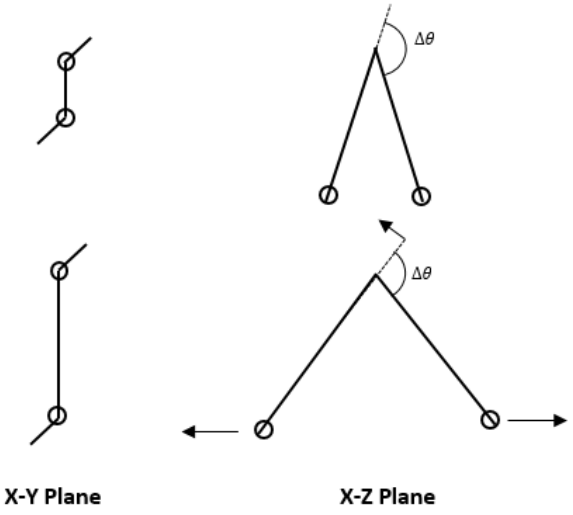

Figure 14: Possible nature of angle variation with relation to ribbon shearing.

This decreasing trend was not noted during the fitting procedure. Indeed, $\Delta\phi$ was treated as

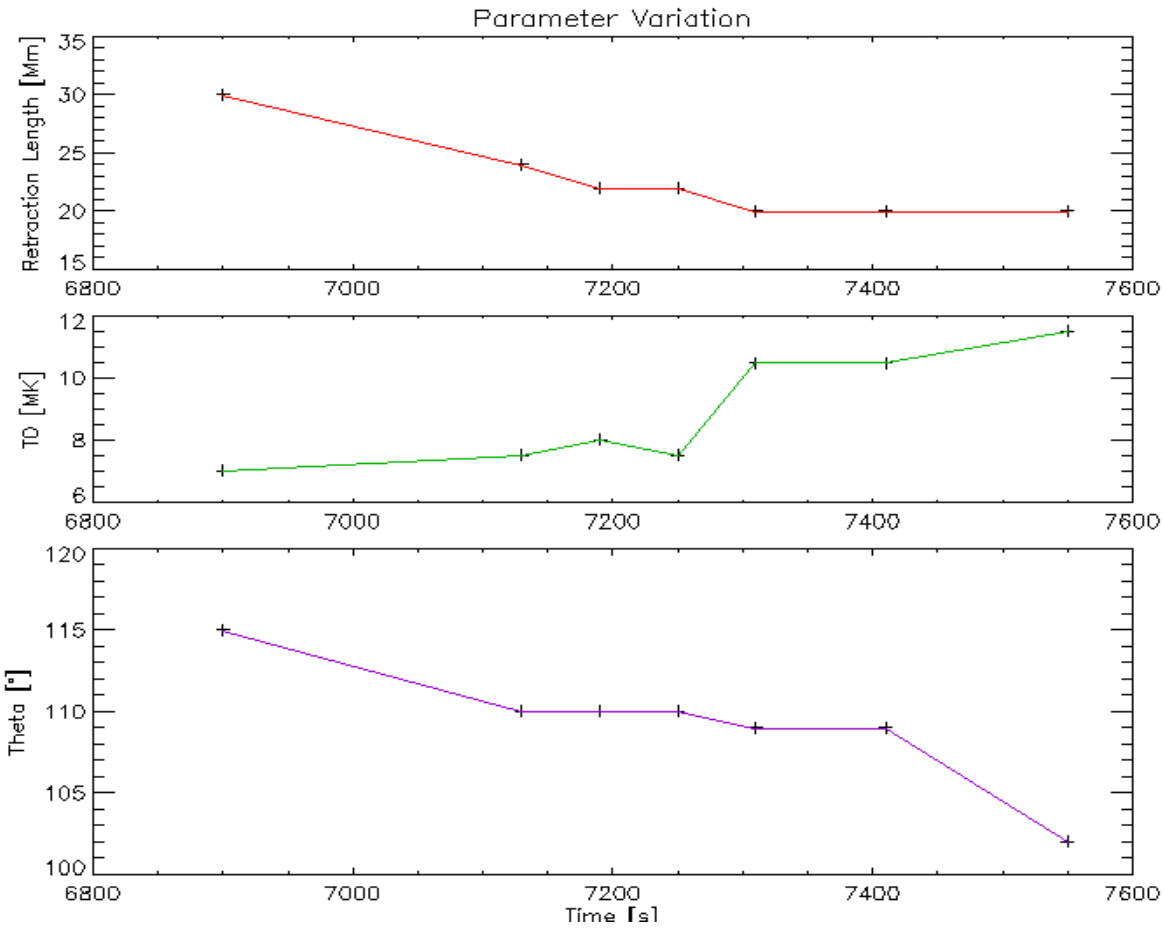

Figure 13: The parameters used plotted at the times they proved to have an effective fit.

somewhat of a fine tuning parameter used to enact small corrections at the higher energies. Thus it is of interest that a clear negative correlation exists as the TFT becomes less bent over time. There are many theoretical constructs which would allow such behaviour. Indeed if we consider an increasing ribbon shear over the course of the flare then the geometry change may manifest itself in $\Delta\theta$ as the connections spread out. However it must be remembered that $\Delta\theta$ is fundamentally different form the ribbon shear commonly discussed. A simple schematic in figure 14 conveys this concept. Another possibility is the idea that over the course of a non-eruptive flare a current sheet retracts towards a null point implying a decreasing magnetic field strength. If the guide field component is assumed to stay constant then this implies the z-component of B must decrease and hence via simple geometry the angle $\Delta\theta$ will also decrease.

7.3 Length

Here we see that as the flare evolves the change in length ΔL decreases. This is consistent with the model of a growing post flare arcade whereby later loops retract less from the diffusion region to the top of the forming arcade. See the diagram of such a 2D setup in figure 15. It should be noted at this point that although ΔL fits this picture, the final lengths L_f are not temporally ordered from low to high. However, since ΔL ultimately controls the magnetic energy release, this is deemed more important than the individual initial or final lengths. These only play a role via the length scales set up which define the loop top-chromosphere information propagation time scales. Thus it should be possible to find effective spectral fits which demonstrate the same decreasing ΔL trend but also show consistent final length ordering. This would bring our model in line with observations which do exhibit an increasing plane of sight final loop length for this event.

In summary we find that the parameter trends observed are possible within the context of flare models. However, we also recognise that many of the processes at work in such events are poorly understood and not consistently predictable. Thus this discussion needs further investigation and

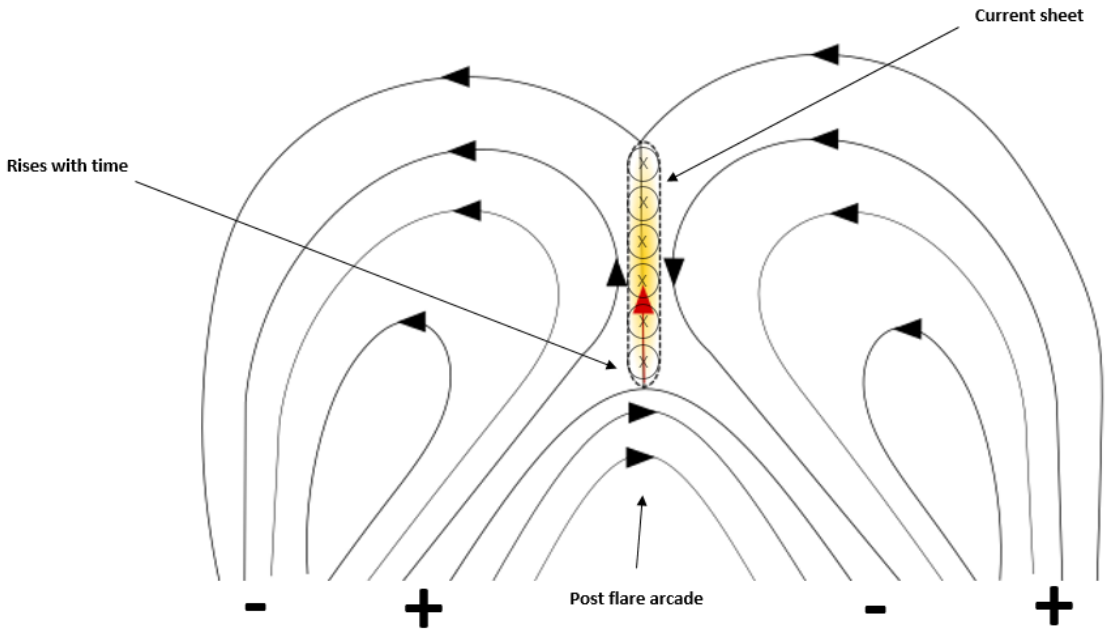

Figure 15: A typical diagram illustrating a 2D non erutive flare setup. As the current sheet shrinks and the post flare arcade grows the change in loop length decreases.

observational support to make firmer conclusions. Nonetheless the strongest trend of apex temperature and density enhancement did seem to be an unavoidable requirement to achieve good spectral fits. Hence it is likely that this is a real effect and efforts should be directed towards finding a potential mechanism.

8 Length Ordered Results

Motivated by the previous discussion we now set about demonstrating that PREFT runs can be found which show a growing L_f ordering with time. The new parameter choices which provide a good fit and length ordering at the seven times are shown in table 5 below. Again we see that the same parameter trends are present and the LRMSD are suitably low to proceed with the multi convolution method. Again the higher values at the lowest and highest times are due to non thermal effects and observational noise respectively.

Performing the multi convolution RHESSI and GOES synthesis, we again see pleasing results as shown in figure 16. The single loop used in the LRMSD comparison now corresponds to the new parameters chosen to fit the time 7250s. As before we see that the multi loop method has a reduced error over the majority of the run with particular improvements at the beginning and end of the impulsive phase. The GOES data also shows a very good fit throughout. This reiterates the previous success of the method and also demonstrates the claim that length ordering should be possible.

9 Discussion

This study has improved our understanding of the spectral response to parameter variations within the PREFT model. This is key for future investigations as now there is well established physical intuition underpinning the changes in synthesised spectra.

1. Increasing T_{apex} results in a softening pivot of the spectra.
2. Increasing ΔL translates the spectra upwards with an enhanced effect at the higher energies.
3. Increasing $\Delta\theta$ results in a hardening pivot and slight upwards translation of the spectra.

Using this to inform our PREFT runs we then proceeded to find parameters which produced single loop spectra offering good fits at different times. These were then incorporated into the multi convolution method. Each single loop light curve per unit flux was convoluted with a share of the total flux transfer rate. Summing the results gave us the net spectrum. This compared favourably with observations, proving a better match to both RHESSI and GOES data. This could be extended further in the future by incorporating more loops at different times and also triggering the coincident collapse of multiple loops at the same time. This would bring us closer the the complex mixture of loops observed in real flares.

Table 5: L_f Length ordered run parameters

Time (s)	L_0 (Mm)	L_f (Mm)	ΔL (Mm)	T_{apex} (MK)	$\Delta\theta$ (°)	LRMSD
6900	80	50	30	6.5	115	0.1433
7130	74	50	24	7.5	110	0.0548
7190	77	55	22	8.3	110	0.0610
7250	79	57	22	8.5	110	0.0597
7310	80	60	20	10.5	109	0.0353
7410	80	60	20	10.5	109	0.0502
7550	85	65	20	12.0	102	0.1546

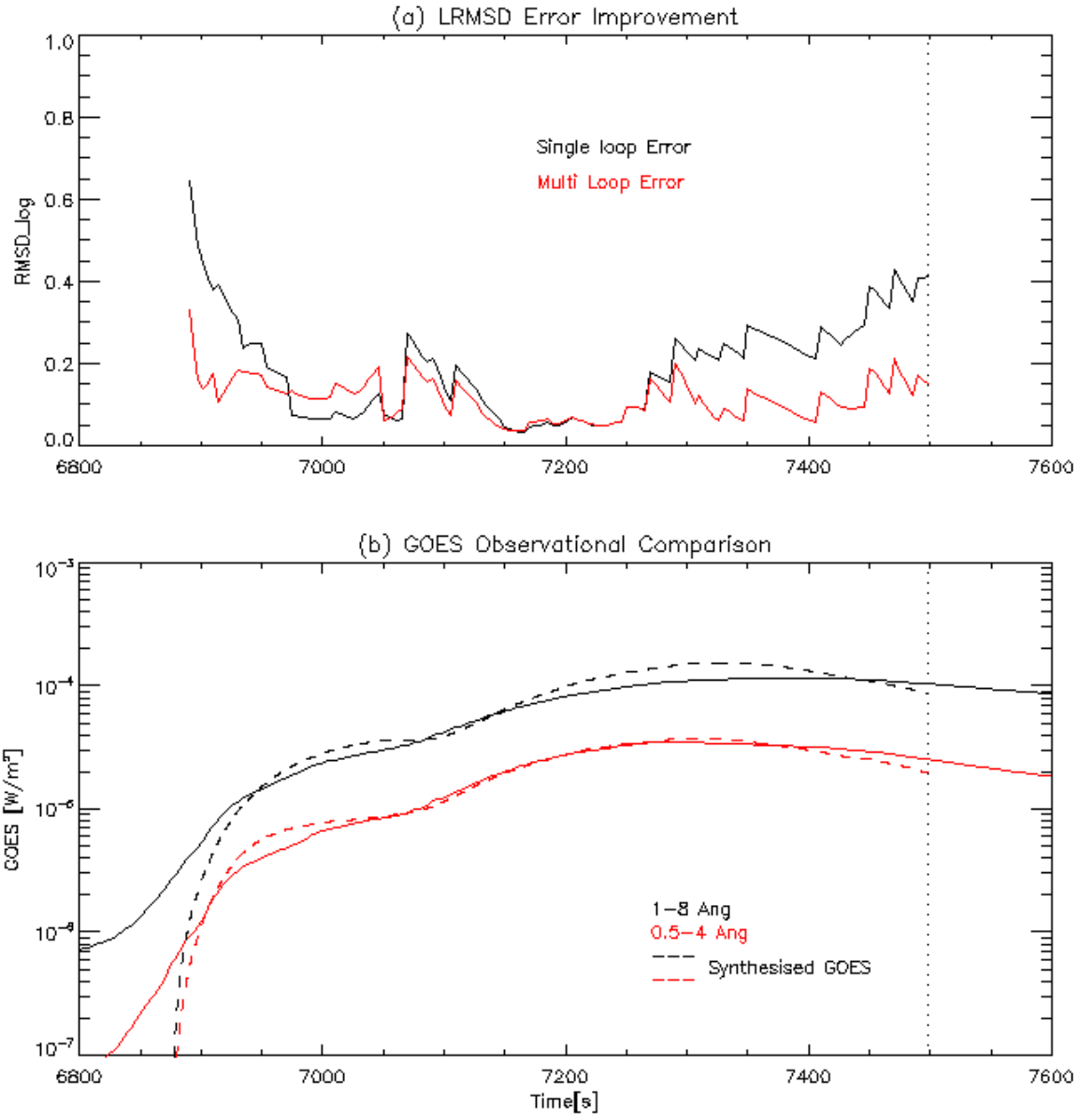

Figure 16: Length ordered multi convolution results. (a) LRMSD for the red line multi convolution method vs the single loop black line method. (b) GOES synthesis observational comparison.

By examining the parameter trends required for effective fitting we see that the evolution of loop types is generally consistent with simple flare models. However, we do note that the most prominent trend is the requirement of high initialisation temperatures and densities at later times to achieve the observed softer spectra and overall increased emission across the two GOES channels. This strongly implies the existence of some mechanism which drives density enhancement at the loop top throughout the impulsive phase.

Further efforts should be made observationally and theoretically to understand if this enhancement is indeed a real physical phenomenon rather than an artefact from an incomplete model.

Acknowledgements

Many thanks to Montana State University for facilitating my research and the NSF Research Experiences for Undergraduates programming for granting financial support. Special thanks also to my advisor, Professor Dana Longcope, for his continued guidance throughout the project.

References

S. E. Guidoni and D. W. Longcope. Shocks and thermal conduction fronts in retracting reconnected flux tubes. *The Astrophysical Journal*, 718 (2):1476, 2010. URL `http://stacks.iop.org/0004-637X/718/i=2/a=1476`.

D. Longcope, J. Qiu, and J. Brewer. A Reconnection-driven Model of the Hard X-Ray Loop-top Source from Flare 2004-Feb-26. *Astrophysical Journal*, 833:211, December 2016. doi: 10.3847/1538-4357/833/2/211.

D. W. Longcope, S. E. Guidoni, and M. G. Linton. Gas-dynamic Shock Heating of Post-flare Loops Due to Retraction Following Localized, Impulsive Reconnection. *Astrophysical Journal, Letters*, 690:L18–L22, January 2009. doi: 10.1088/0004-637X/690/1/L18.

E. N. Parker. Sweet's Mechanism for Merging Magnetic Fields in Conducting Fluids. *Journal of Geophysics Research*, 62:509–520, December 1957. doi: 10.1029/JZ062i004p00509.

H. E. Petschek. Magnetic Field Annihilation. *NASA Special Publication*, 50:425, 1964.

R. Rosner, W. H. Tucker, and G. S. Vaiana. Dynamics of the quiescent solar corona. *The Astrophysical Journal*, 220:643–645, March 1978. doi: 10.1086/155949.

P. A. Sweet. The Neutral Point Theory of Solar Flares. In B. Lehnert, editor, *Electromagnetic Phenomena in Cosmical Physics*, volume 6 of *IAU Symposium*, page 123, 1958.